

CERN

H8 data analysis procedure of crystals tested during Oct.13th and Dec.10th 2014 Test Beams

Federica Andrisani
January 19, 2015

INTRODUCTION

UA9 collaboration main goal is to demonstrate that channeling of charged particles in a bent crystal can be used as a technique to steer ultra-relativistic beams with high efficiency in order to improve the collimation of both proton and heavy ion beams at the LHC. Measurements of suitable crystals have been carried out in a fixed target experiment set in the CERN North Area: the external H8 beamline. Here the different crystals made by the groups of INFN Ferrara, PNPI (Saint Petersburg) and IHEP (Protvino) are installed and tested to verify some fabrication parameters such as the torsion and the bending angle.

The study of channeling phenomena requires very accurate angular alignment of the silicon crystals with respect to the beam, as the critical angle for channeling, i.e. the angular acceptance of incident particles with respect to the crystalline planes, is of the order of $10 \mu\text{rad}$ for $400 \text{ GeV}/c$ protons. The measurement approach relies on precise single-particle tracking with high-resolution silicon microstrip detectors called telescope, whose angular resolution for $400 \text{ GeV}/c$ protons is about $5.2 \mu\text{rad}$.

Once the alignment is successful, the crystal is installed on the goniometer and moved into the beam with different orientations to find the best position for channeling. Then, this orientation is fixed and a run of high statistics is started, in order to collect few tens of millions events needed for the offline analysis.

This report presents a detailed description of the technical procedure and preliminary data analysis of the crystals tested during both the October and December 2014 Test Beams, taking into account that a secondary pion beam of $180 \text{ GeV}/c$, with a consequent telescope angular resolution worsen to $\approx 12 \mu\text{rad}$, was used.

Five silicon crystals were tested in October and four of them were analysed:

- Strip crystals from INFN Ferrara: ST9 (old SPS crystal) and ST76 (LHC type)
- Quasi-Mosaic crystals from PNPI: QM33 (LHC type) and QM36 (SPS type)

Instead, in December, five multi-strip crystals and two more simple crystals were measured and analysed:

- Multi-strip from INFN Ferrara: MSTF-13
- Multi-strip from IHEP: MSTI14-2, MSTI14-4, MSTI14-5, MSTI14-6
- Strip crystal from INFN Ferrara: ST76 (LHC type: re-measured)
- Quasi-Mosaic crystals from PNPI: QM38

CRYSTAL MEASURING

The data collected during the Test Beam are then processed and formatted within the XDAQ (Data Acquisition system) online framework, to be then stored in the standard CMS data format, so that they can be processed both online and offline using the CMS software environment (CMSSW). Later on, they are reconstructed and converted to files .root, in order to be easily analysed offline by the data analysis program ROOT. ROOT is an object-oriented C++ -based software developed by CERN.

In the following description of a typical procedure for crystal measuring during a test-beam, a left-handed coordinate system is adopted, with the z-axis indicating the beam direction, while x and y axes refer to the horizontal and vertical displacements. The crystals used for channeling studies are usually oriented so that the expected displacement is in the horizontal plane, so the angular scan is about a vertical axis.

Alignment run

After each intervention in the beam area or every time a crystal is substituted, dedicated runs are used to collect a few 100,000 events tracks before the alignment parameters are extracted, in order to refresh the reconstruction algorithm and verify that the telescope is correctly working.

The alignment procedure is extremely important and it is used to calculate possible misalignments within the tracker planes. Only events with a single track hit in each sensor are selected.

The tracker detector is composed by five XY-planes; between them, the fourth plane is 45° rotated to solve ambiguities in the reconstruction from multiple outgoing tracks.

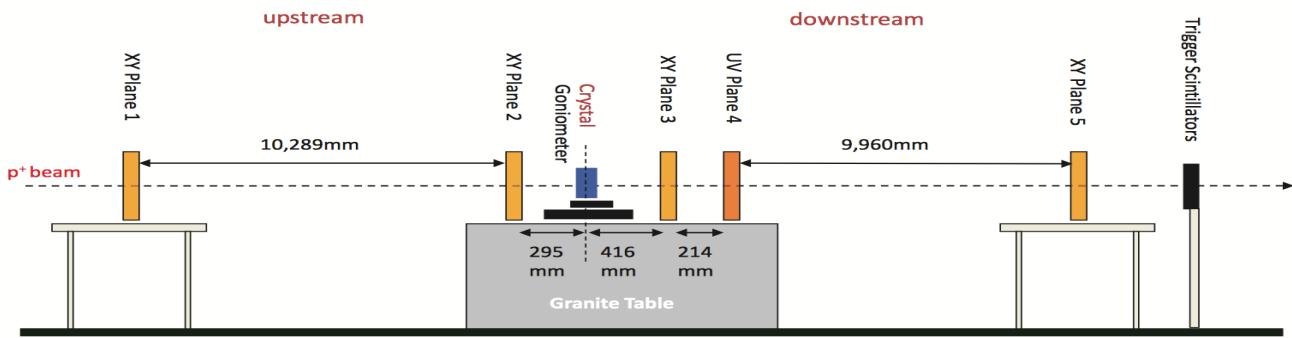


Figure 1. Experimental layout in the H8 beam line. The UV plane denotes the 45° rotated XY-plane.

Since the planes are well-separated one from the others, the procedure must take into account the offsets in the plane orthogonal to the beam.

1st and 5th planes are used as reference: straight line tracks are interpolated in (x,y) directions to the intermediate planes and the hit residuals are measured. Of course, hits from the 4th plane must be rotated of -45° along z-axis.

As shown in Figure 2, the (x,y) origin of the system is chosen to lie in the centre of the beam spot, while an offset is applied to the last plane so that the average track direction is zero.

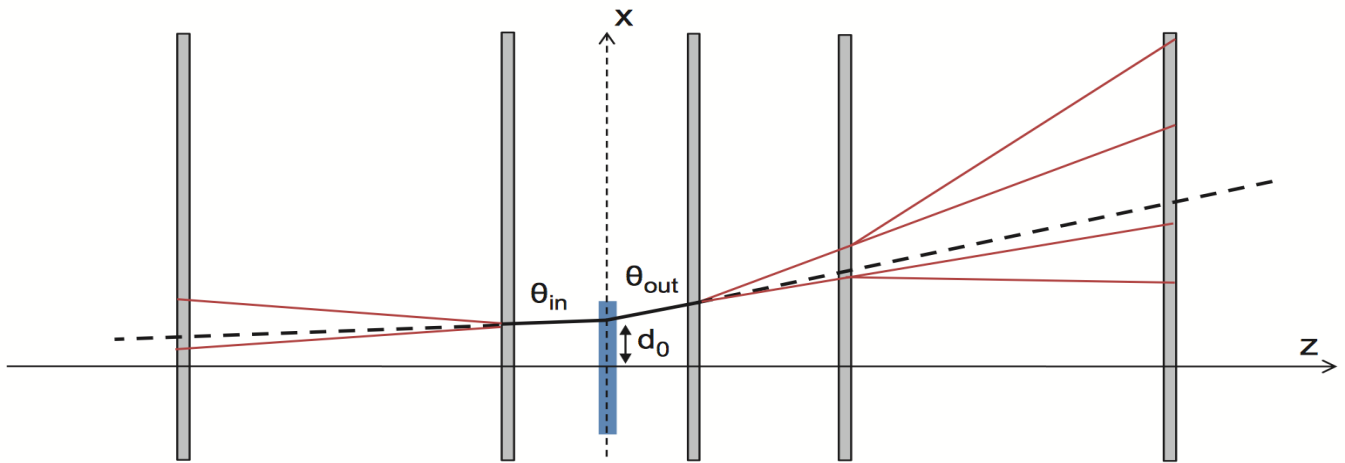


Figure 2. Track fitting method where θ_{in} and θ_{out} are respectively the incoming and outgoing angle (solid black lines) while d_0 is the impact parameter at the crystal.

Rotational misalignments of the sensors about the z-axis can also worsen the effective resolution, amounting to interdependence between the impact point along the strip direction and the estimated hit position. The rotational misalignment (“twist angle”) of each sensor can be overcome by applying iterative corrections until the XY correlations are eliminated. Such rotational misalignments were measured to vary between 0.1 ÷ 8 mrad.

The alignment procedure converges within a few steps and can achieve a precision of <1 μm for the relative offsets and <0.1 mrad for the twist angles.

Angular Scan run

Before an angular scan run starts, the crystal is first installed on the goniometer (or repositioned into the beam if already mounted) and then moved to find the best transversal position for channeling. The aim is to have the beam hitting the center of the crystal.

After laser pre-alignment, a fast scan of the crystal angular position is performed measuring proton tracks with the parallel plate chamber, thanks to the high particle rate that it can sustain. A $10\text{--}20\mu\text{rad}$ rotation of the crystal is performed every accelerator cycle and a profilometer device records the corresponding beam profile downstream of the goniometer. This procedure is able to define, precisely and in a short time, the channeling angular position and the total angular range to be measured with higher statistics runs with the silicon detectors.

A more detailed scan is then performed with least angular steps of $3\text{--}5\mu\text{rad}$, recording silicon detectors data for about 10–15 accelerator cycles for each crystal position, in order to collect enough statistics for the offline data analysis.

The enlargement produced by multiple scattering in the crystal on the outgoing angular distribution says whenever the crystal is passing through the beam and Medipix detectors are meant to observe it.

Thanks to Medipix, different fast angular scans are performed by rapidly moving the goniometer, in order to find channeling and other main effects orientation. Channeling appears as the incoming beam splitting in two outgoings. The pictures on the right show the online angular scan of the crystal QM36 installed on the goniometer.

From the second plot, it is possible to recognize the channeling spot at approximately $175\mu\text{rad}$.

Apart from channeling, other important and interesting effects can occur, such as dechanneling, volume capture (VC), volume reflection (VR) and amorphous.

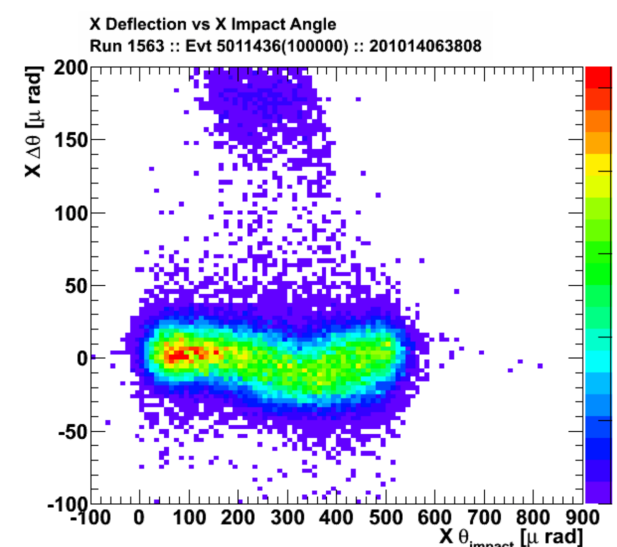
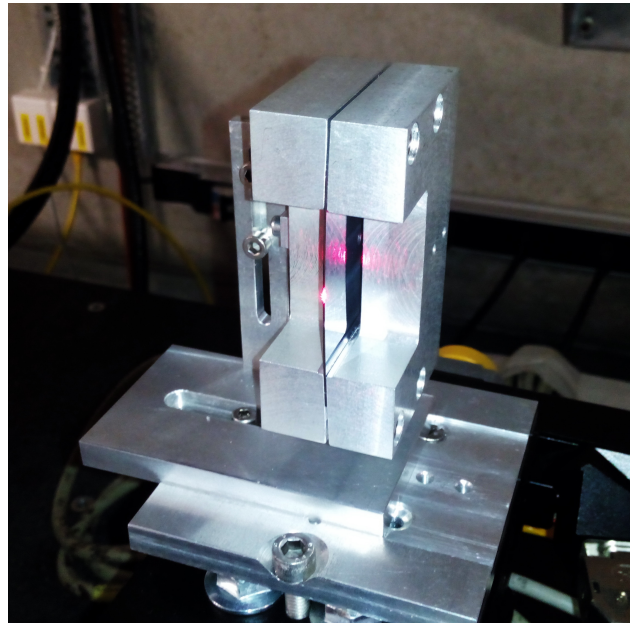


Figure 3. QM36 installed and aligned with laser beam (up) and its angular scan online picture (down)

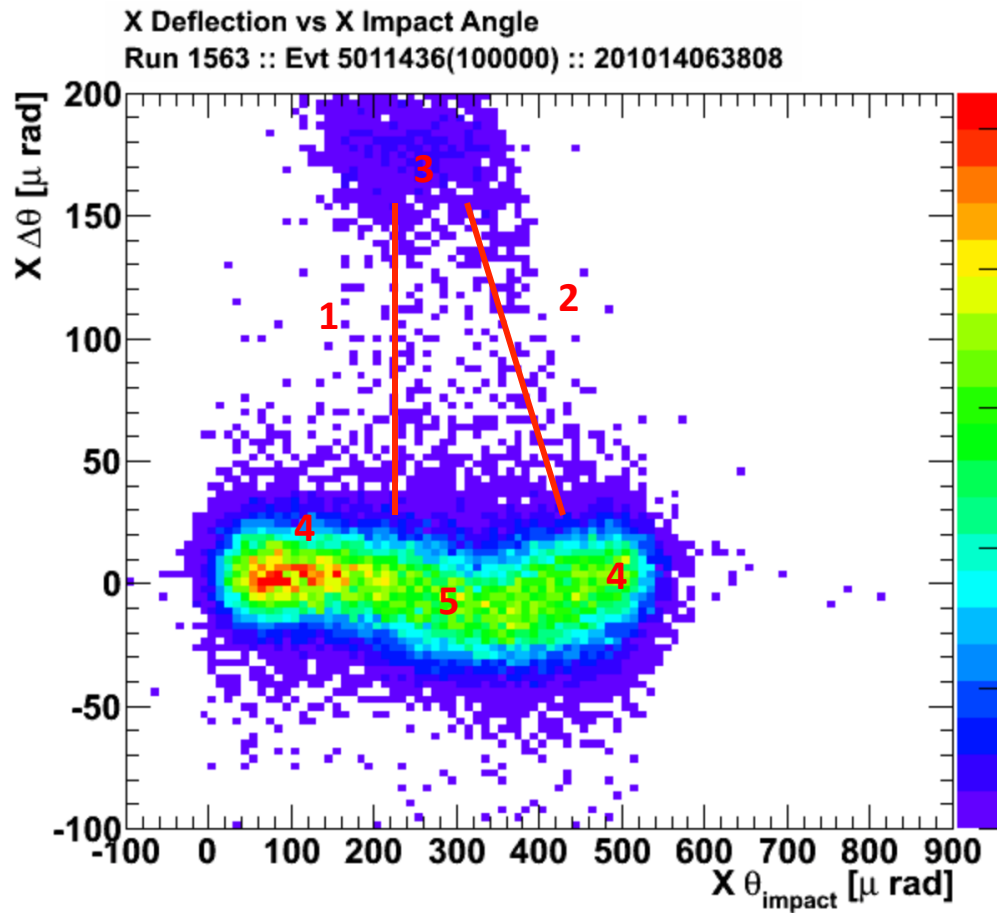


Figure 4. Angular scan of QM36; the 5 main effects that may occur are indicated in red:

1. Dechanneling
2. Volume Capture
3. Channeling
4. Amorphous
5. Volume Reflection

The channeling peak is separated from the unperturbed beam by $\sim 175 \mu\text{rad}$, which corresponds to the crystal bending angle (measured with optical techniques) within experimental errors. By increasing the goniometer angle, the channeling condition is met: most of the particles are captured in the crystalline planes and steered outward, resulting in the zone (3) of the plot above.

A small fraction of the initially channeled particles are “dechanneled” due to an increase of the transverse energy, as it is visible in region (1).

The volume reflection region (5) appears when the goniometer angle is further increased; the particle enters the crystal with a too high transverse energy for being channeled and, somewhere inside the crystal, the particle trajectory becomes almost tangent to the bent crystalline planes. Here two phenomena may occur: the particle is channeled within the volume of the crystal (Volume Capture, 2) or, as an alternative, the transverse momentum of the particle can be reversed like in a scattering process with a potential barrier (Volume Reflection, 5). This last region extends over a wide angular area and almost the whole beam is displaced with respect to the unperturbed beam, in the opposite direction respect to the channeling spot. In region (4) volume reflection is no longer possible and the crystal is crossed by the incoming particles in an amorphous orientation.

High Statistics run

Once the angular scan is computed, the crystal position is fixed in correspondence of a specific effect to be analyzed. Usually, they are done in channeling orientation, but the amorphous and the volume reflection ones are possible as well.

The crystal characterization in such condition is crucial to determine the best performance of a collimation system based on bent crystals.

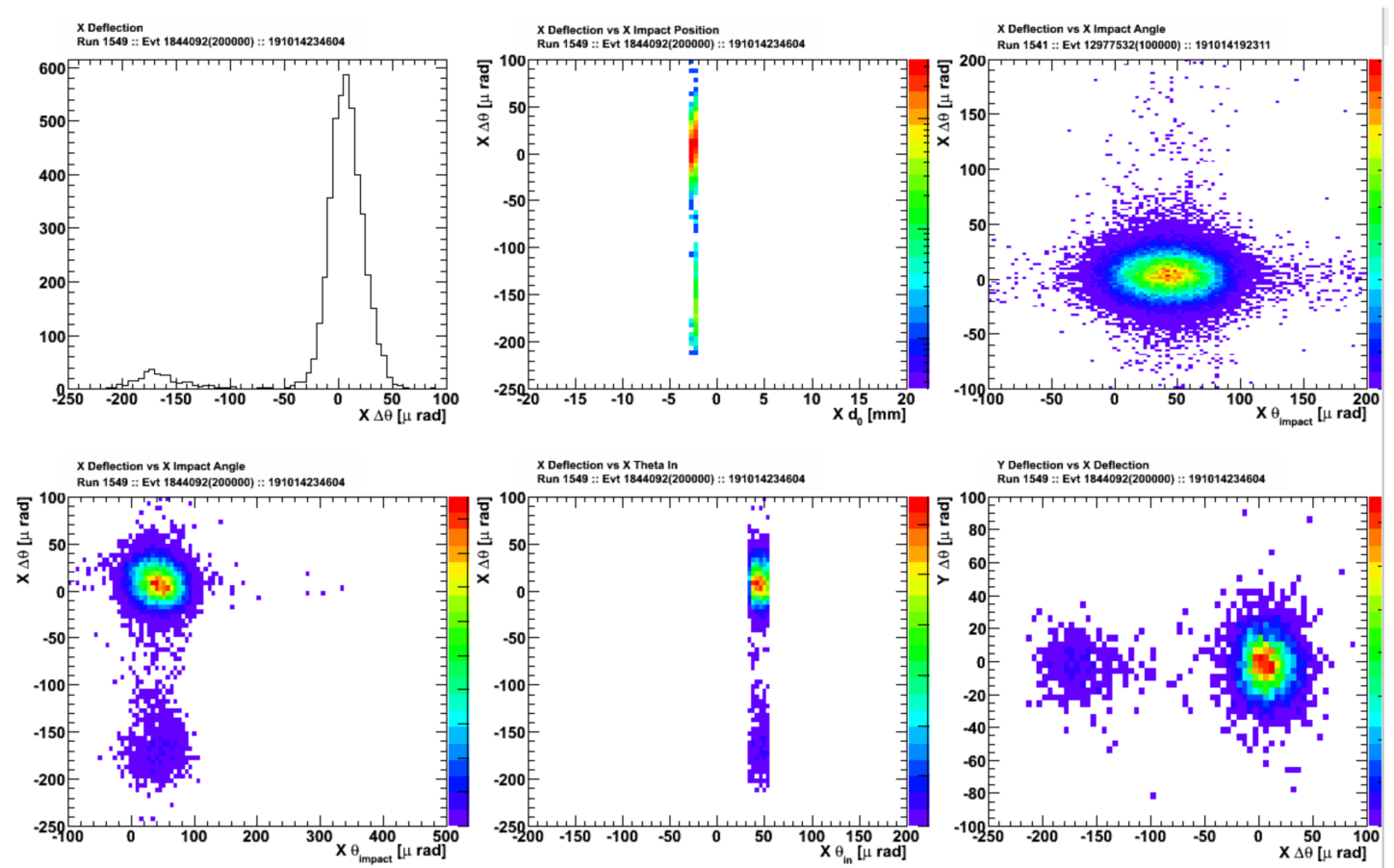


Figure 5. High statistics plots for QM36 in channeling orientation. They show in particular a 1D-histogram (1plot, first line) for the deflection angle and a 2D-histogram (1plot, second line) for deflection angle versus impact angle, both presenting a clear separation between channeling and amorphous phenomena.

BEAM PROPERTIES – October run

The Alignment run analysis

Previously, it has been explained how the Alignment run is used for the tracker calibration, in order to guarantee a correct data reconstruction, but now, talking about the data analysis, this run is needed to verify that the following data have been registered without any problem. For instance, if the telescope resolution is higher than the expected one ($5.2\mu\text{rad}$ for protons at $400 \text{ GeV}/c$) it could mean that the beam is intercepted by something that is not supposed to be there and that adds a contribute to the multiple scattering.

When this happens, the reconstruction algorithm is not reliable anymore and the runs that comes after such alignment run can't be used, since the tracks have been wrongly reconstructed.

Moreover, the main beam parameters are controlled.

During the October 2014 Test-Beam, the UA9 experiment had the use of a pion beam of $180 \text{ GeV}/c$ instead of a proton beam of $400 \text{ GeV}/c$.

The beam parameters (reported in **Fig. 6** and **Fig. 7**) remained almost constant during the whole testing period; the beam spot was quite large, with 3.347 mm and 1.589 mm width in x - and y - directions respectively, while the beam x -divergence was huge, i.e. of $25.86\mu\text{rad}$. Instead, the y -divergence had not Gaussian shape and provided a FWHM of about $150\mu\text{rad}$ (**Fig. 8**).

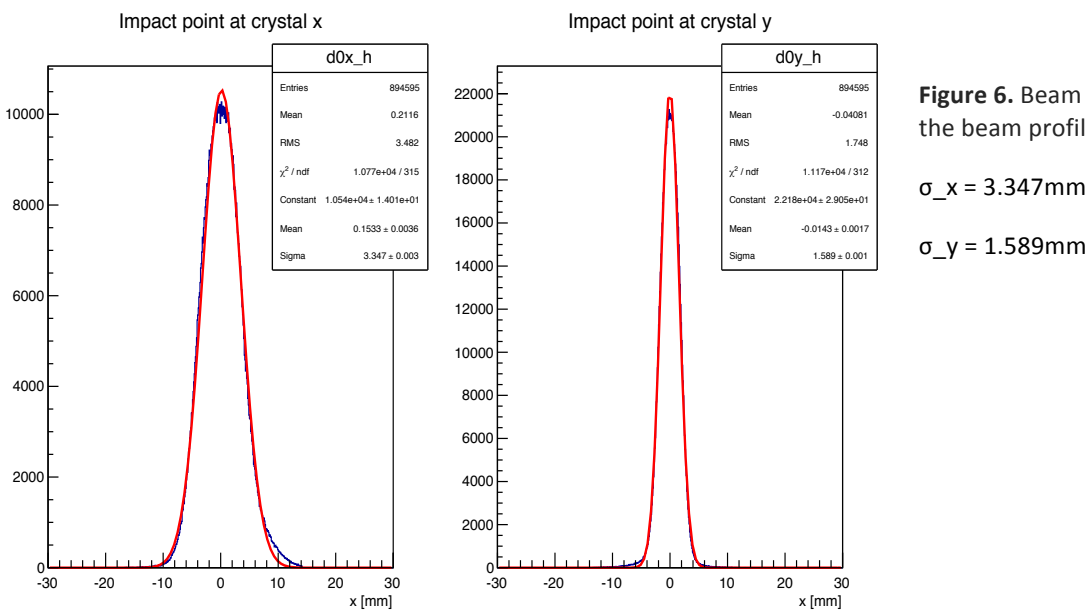


Figure 6. Beam dimensions; $d0_x$ and $d0_y$ indicate the beam profile in x - and y -directions.

$$\sigma_x = 3.347 \text{ mm}$$

$$\sigma_y = 1.589 \text{ mm}$$

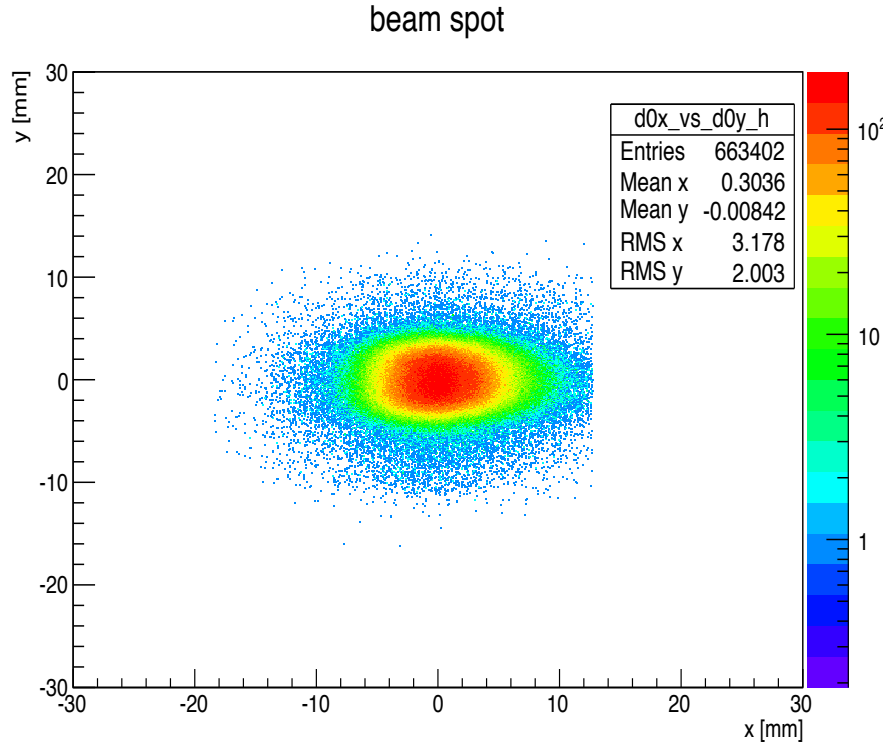


Figure 7. Beam spot 2D-histogram. It is a double Gaussian curve respect to the beam dimensions, where the projections on x- and y- axes give the beam profile of **Fig. 6**

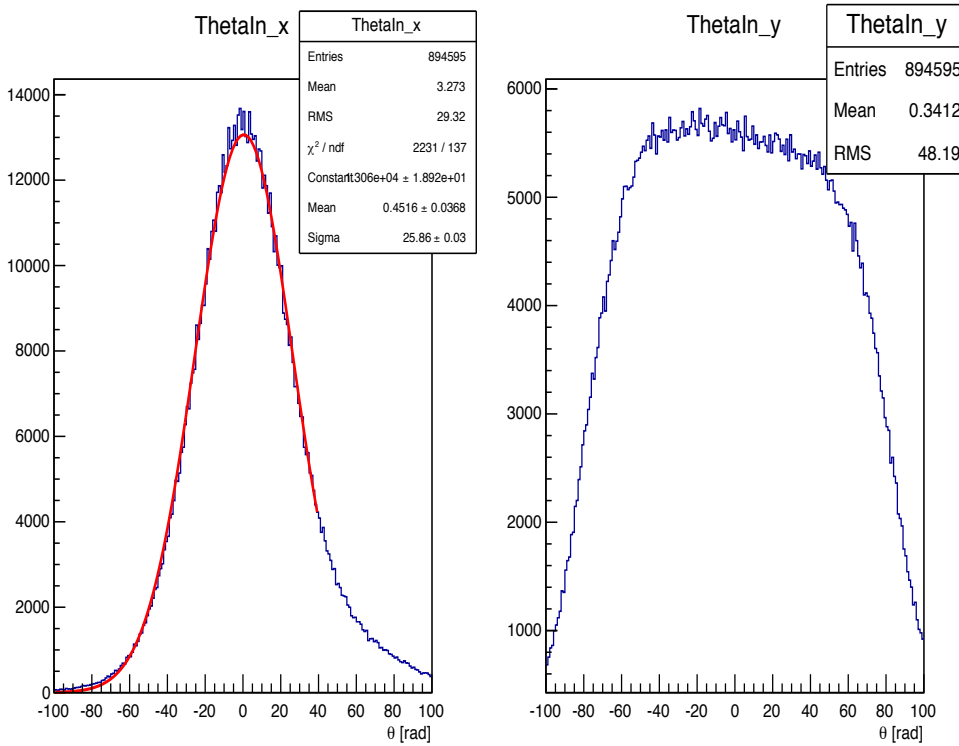


Figure 8. Beam divergence. The non-Gaussian shape of y-plot is evident. This is likely to be due to the optics of quadrupole magnets, as a consequence of our request about reducing the x-divergence. A further reason could be the fact that it was a secondary pion beam.

Another relevant feature is the telescope resolution. In the previous paragraphs, we have seen that for protons at 400 GeV/c the tracker resolution had been calculated to be $\sim 5.2 \mu\text{rad}$, taking into account scattering phenomena due to air in non-in-vacuum sectors of the beam pipe. Instead, with a secondary pion beam, this resolution worsened up to about $12 \mu\text{rad}$, as reported in Fig. 9.

This resolution drop is because the particles energy is lower.

So, the alignment runs are analyzed to inspect how the telescope operates and to verify the beam parameters right after the crystal installation on the goniometer. Only single track events are selected, without applying any geometrical or angular cut.

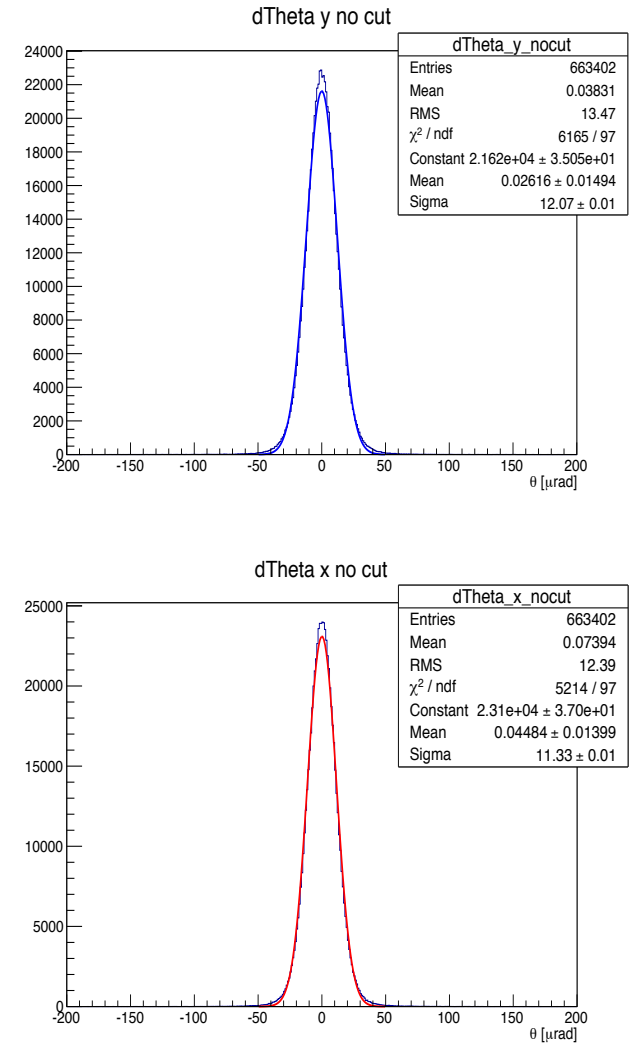


Figure 9. The telescope resolution is the sigma of the deflection $\Delta\vartheta$ given by ($\vartheta_{\text{out}} - \vartheta_{\text{in}}$), in x- and y- directions.

CRYSTALS

Five different crystals were measured during this test-beam run and, for four of them, the same offline analysis procedure has been lead.

Crystal name	Crystal type	Manufacture	Bending angle production [μrad]	Length (z) [mm]	Width (x) [mm]
QM33	Quasi-Mosaic	PNPI	44±2	4	
QM36	Quasi-Mosaic	PNPI	170	0.5	
ST9	Strip	INFN	150	2	0.5
ST79	Strip	INFN	51	4	0.5
QM32	Quasi-Mosaic	PNPI	~175	0.96	

Table 1. Basic information of the crystals analyzed in October 2014 TB

As reported in **Tab.1**, two kinds of crystal were tested: Quasi-Mosaic and Strip crystals. They do have also different characteristics. In fact, while Strip crystal plates are cut and bent to produce an homogeneous anticlastic curvature of the order of few hundreds of μrad , the QM are cut with the external faces parallel to the atomic lattice and bent by hundreds of μrad through the quasi-mosaic elastic effect.

A crystal of each type, respectively produced in Ferrara University and at PNPI, is schematically shown in **Fig.10**.



Figure 10. Schematic pictures of strip (1) and QM (2) crystals are reported to show the different characteristics of these two configurations.

DATA ANALYSIS

In the following pages the analysis path is reported, focusing with a particular attention on the channeling efficiencies and the torsion corrections, which are crucial especially for strip crystals.

High Statistics run analysis

After a fast angular scan, the goniometer is fixed in the optimal channeling position to register some million events for the High Statistics run. The crystal characterization in such configuration is crucial to determine the best performances of a collimation system based on bent crystals. In particular, we want to select at first only the particles impinging on the crystal surface by applying geometrical cuts. Then, to study those effects that occur for particles with the right parameters to be channelled, we need to impose limitations to the incoming angle, in a way that this angle results coherent with the critical angle for channeling of pions at 180 GeV/c.

Concerning the geometrical cuts, there are two different techniques, since we want to distinguish the case of a Strip crystal from that of a QM.

Strip crystals

As reported in **Tab.1**, two strip crystals were analyzed in October. The ST9 is a crystal that was removed from SPS in 2011, while the ST76 is a LHC twin of another strip installed to LHC in February 2014.

In principle, the incoming surface of the crystal is orthogonal to the mean incoming direction of the beam, (except for torsion, that modifies the surface orientation). From this first step analysis, we get four plots representing the particle distribution in function of the four possible combinations of deflection in x- and y- directions towards the impact x- and y-positions. Between these 2D-histograms, the most important is the $\Delta\vartheta_x$ vs $d0_x$, since from it we obtain the crystal dimensions along the x-axis, necessary to proceed with the geometrical cuts (**Fig.11**).

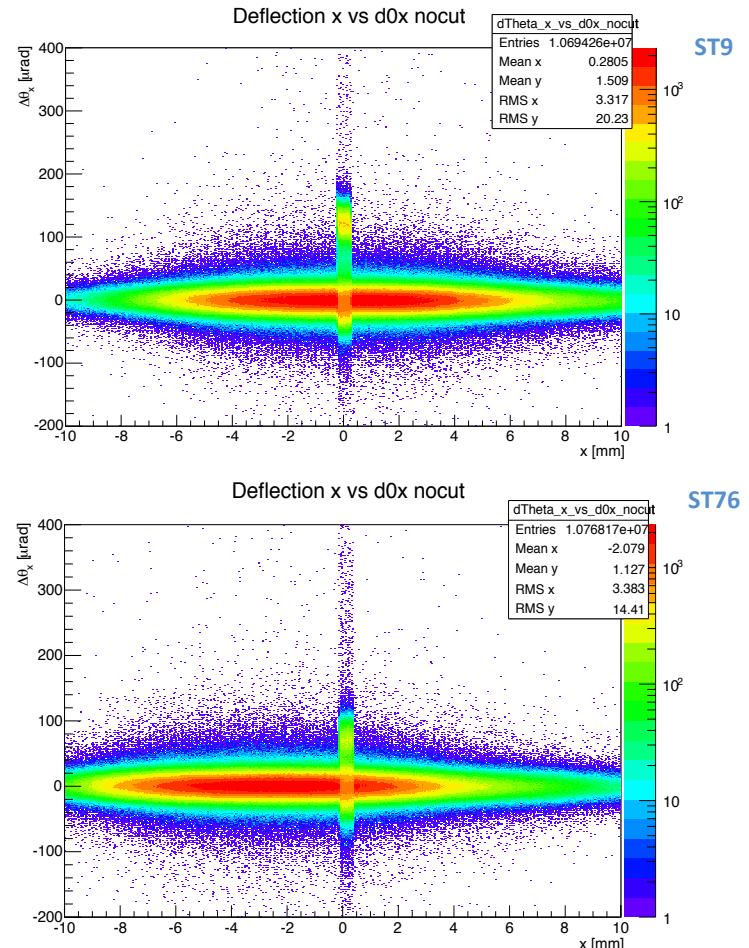


Figure 11. x-Deflection vs x-impact position for ST9 and ST76 crystals.

Here, the enlargement due to the multiple scattering in correspondence of the crystal is clearly visible, as well as the channeling spot. They are both caused by the fact that the crystal intercepts the beam.

Looking at the x-axis of the two plots in **Fig.11**, we can verify that both strips are 0.5mm width, which fits with the crystals dimensions we are examining. On the contrary, for y-dimension we refer to the σ_y of the beam reported in **Fig.6**, computing a final dimension of $3\sigma_y$ in order to select only the core particles, excluding the halo ones (please note that the final value of $3\sigma_y$ is much smaller than the crystal vertical dimension).

Quasi-Mosaic crystals

As for strips, the installation of the crystal in the holder gives a primary curvature and a secondary anticlastic curvature, but for QMs there is also a further effect along x-axis, due to both the different holder used and the rigidity tensor of (111) planes: here, there's a non-null element that provides a curvature along the displacement in function of y. The final effect is a tridimensional deformation of the crystalline planes, that must be taken into account during the analysis, because it basically results in a variation of the incoming angle of the particles respect to the crystalline planes, depending on the impact position on the surface (**Fig.12**). This tridimensional dependence on the curvature exists in strip crystals too, but it can be neglected since it is not as accentuated as for QMs.

That's why it is not possible to use the same technique implemented for strip crystals: we cannot consider all particles indistinctly, since the relative angles between the particles and the crystal lattice provide deflections in function of the impact point which are pretty similar to an angular scan.

The incoming surface in QMs is bigger than the beam spot, therefore sometimes the whole beam hits the crystal front-face, while in other cases we need to select only the particles that have interacted with the crystal, recurring to the same method described for strip crystals.

Once the geometrical cuts are actuated, it is possible to compute the channeling efficiency in function of the impact point in (d_{0x}, d_{0y}) , where we select the biggest area in which the efficiency is approximately constant and the highest possible (**Fig.13**): here, the incoming surface can be approximated as flat and its dimensions are used to define the geometrical cuts like those found for strips. This method allows leading a coherent analysis for both crystal types.

Channeling efficiency is defined as the number of channeled particles respect to the number of total particles in function of the impact point (x, y) .

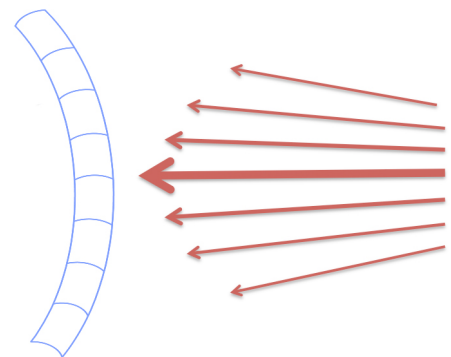
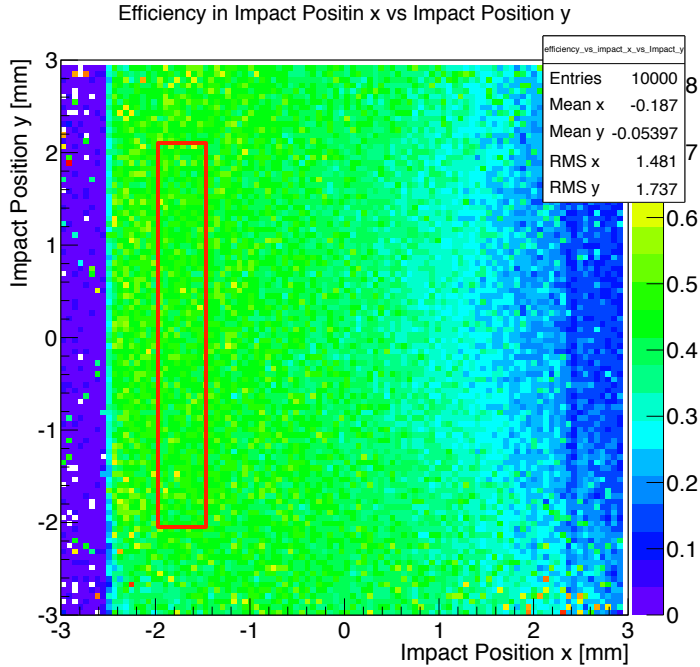


Figure 12. Scheme of the interaction between the impinging beam ad the QM surface



The crystal curvature makes the efficiency depending on the impact position d_{0x} , identifying a central area where the channeling efficiency is constant and so we can approximate the crystal surface as flat.

In **Fig.13**, the red-border contains the particles we want to consider in the coherent effects analysis. Its dimensions along x- and y-axes are used to select the geometrical cuts, needed in order to have a comparable analysis for both strips and QMs crystals.

Figure 13. Channeling efficiency in function of impact position in x- and y- directions for QM33. The red border underlines the area where this efficiency is maintained constant: min_x= -2mm, Max_x= -1.5mm, min_y= -2mm, Max_y= 2mm.

Torsion analysis and correction

Strip crystals are likely to present one more effect that deforms the crystal inducing a rotation along the vertical structure. It results in a different relative angle between the particles and crystalline planes directions. This difference is a linear function of the vertical coordinate. So, torsion is presented as a relative rotation along y-axis of two crystal sections, taken at different heights of the same axis. Such phenomenon is extremely important and it must be corrected during the offline analysis, because it influences the channeling condition of particles themselves and it means that the ideal channeling condition varies with the d_{0y} point of impact on the surface. It is then possible to measure the torsion through a peculiar definition of channeling efficiency that counts the number of channeled particles respect to the total number of particles that have interacted with the crystal per vertical length unit.

From the plot of efficiency in function of impact angle in x and impact point in y, we extract the behavior of the impact average angle ϑ_{rel_x} , or rather the most efficient angle respect to d_{0y} . The linear regression (an example is reported in **Fig.14**) returns the torsion [$\mu\text{rad}/\text{mm}$] as the slope of the line, while the abscissa is the offset angle that brings the relative angle in 0.

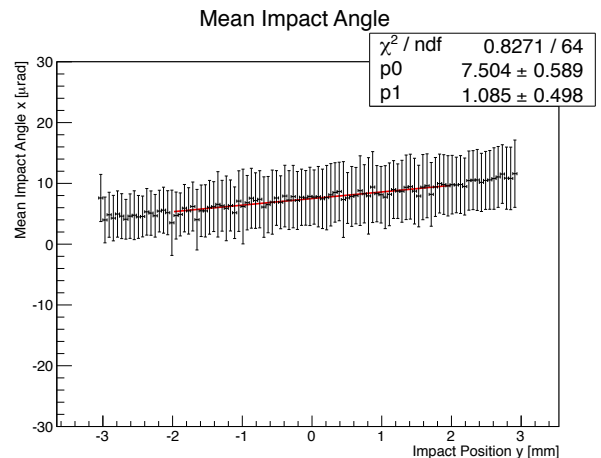


Figure 14. Linear regression for ST9; p_0 is the impact angle offset, while p_1 is the crystal torsion.

Channeling efficiency

To obtain the channeling efficiency histogram, we need to apply first the angular cuts mentioned in the previous paragraphs. Of course, they must be coherent with the critical angle and with the telescope resolution. They are applied to the deflection versus impact angle (both in x-direction) plot and, for protons at 400 GeV/c, they are equal to $\pm 5 \mu\text{rad}$ and $\pm 10 \mu\text{rad}$, i.e. equal to half and a total critical angle.

Even if during this test beam we had pions at a lower energy, the cuts that have been applied remain the same.

The following plots show these two cases of efficiency for each crystal that was measured in October 2014, where in red we have the Gaussian fit for the channeling peak taken on the mean channeling angle. We define channelled particles all those particles that belong to an angular range of $\pm 3\sigma$ from the Gaussian center of the channeled beam.

ST9:

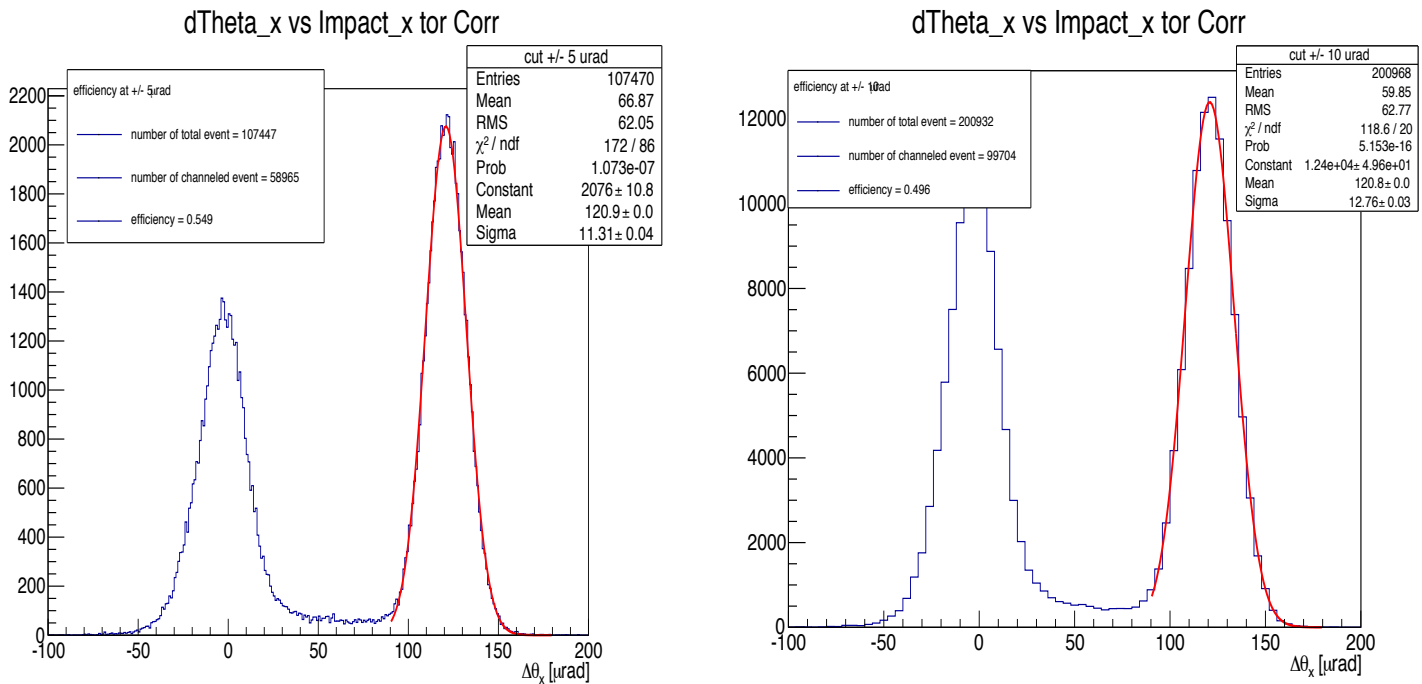


Figure 15a. Efficiencies for $\pm 5 \mu\text{rad}$ and $\pm 10 \mu\text{rad}$ cuts of ST9 crystal: 0.549 and 0.496 respectively.

ST76:

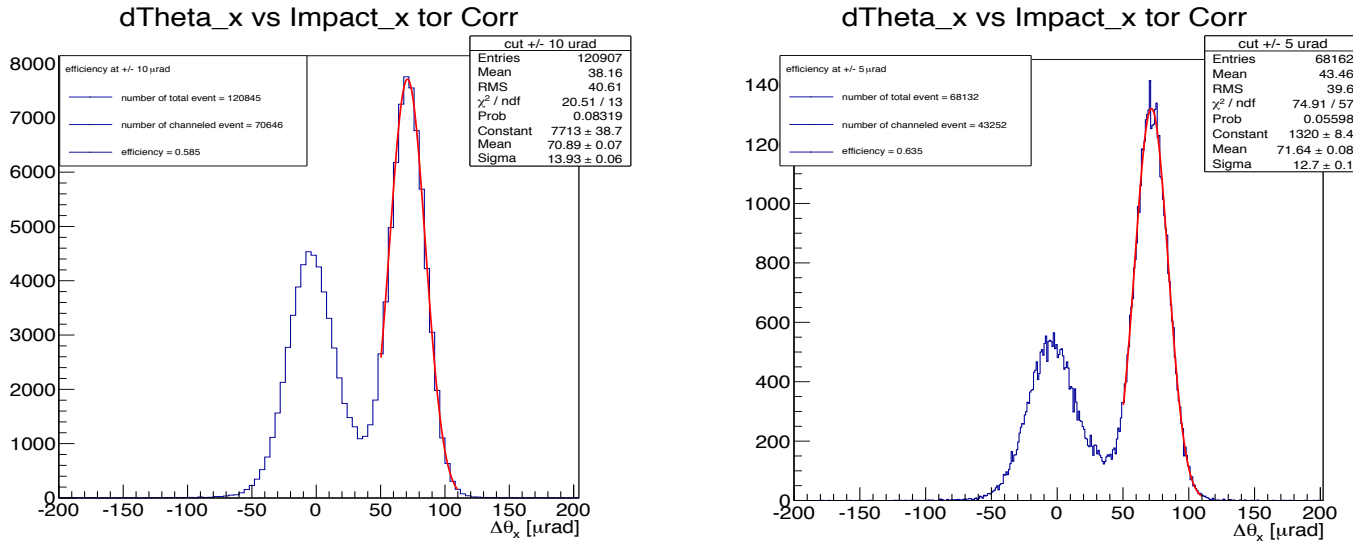


Figure 15b. Efficiencies for $\pm 5 \mu\text{rad}$ and $\pm 10 \mu\text{rad}$ cuts of ST76 crystal: 0.585 and 0.635 respectively.

QM33:

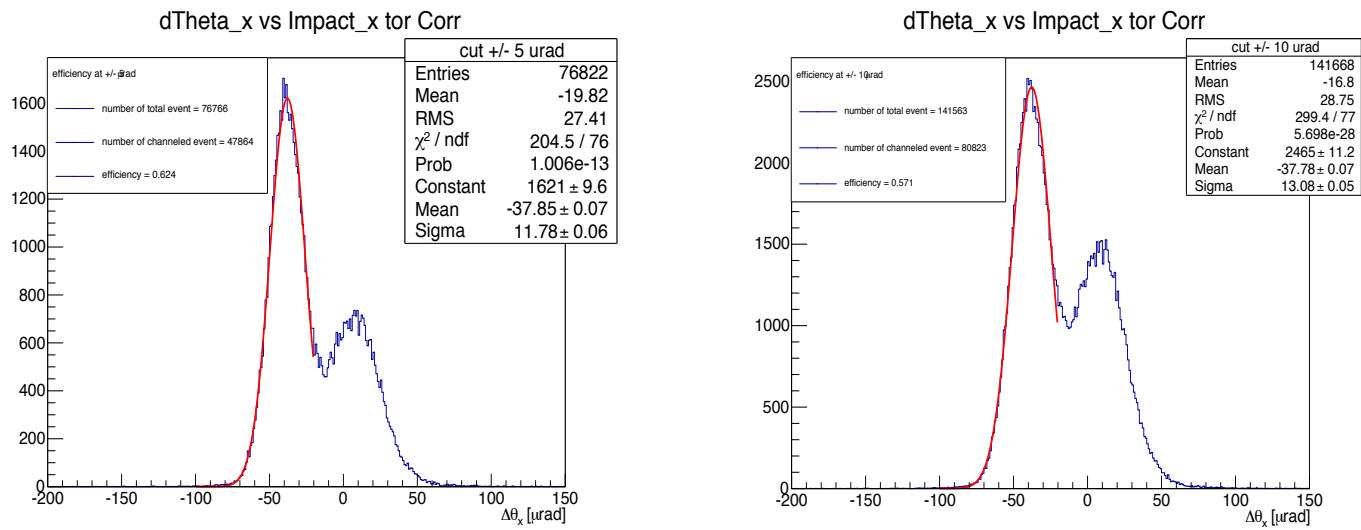


Figure 15c. Efficiencies for $\pm 5 \mu\text{rad}$ and $\pm 10 \mu\text{rad}$ cuts of QM33 crystal: 0.624 and 0.571 respectively.

QM36:

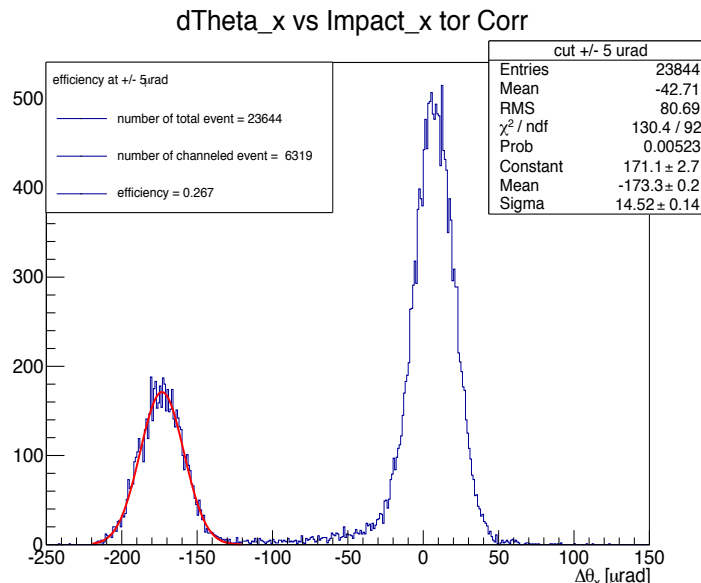
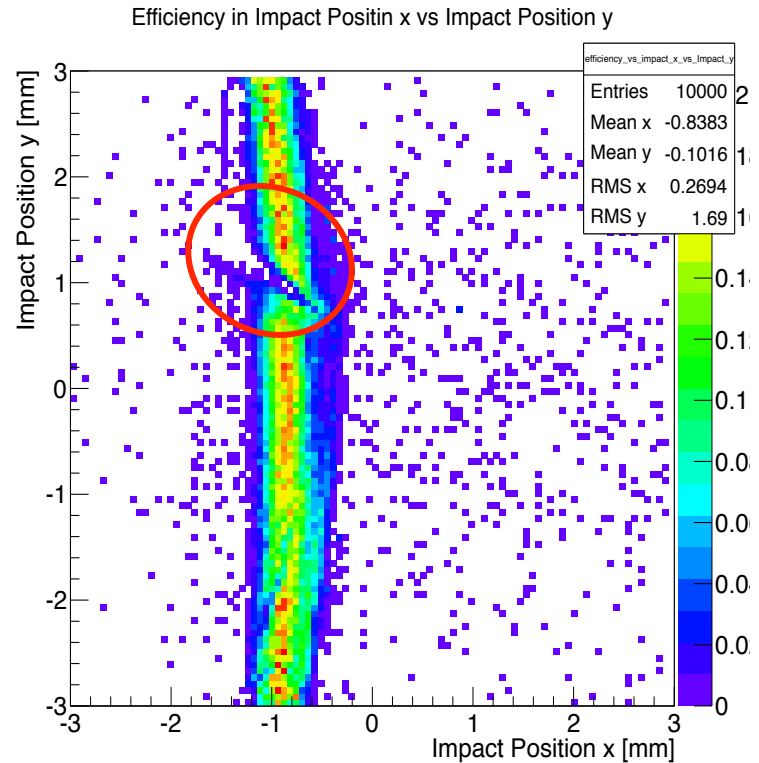


Figure 15c. Efficiency for $\pm 5 \mu\text{rad}$ cut of QM36 crystal: 0.267. This channeling efficiency is much lower if compared to the other crystals described in this report, because of the lack of channelled events in correspondence of $y = 1\text{ mm}$. As visible in the 2D-histogram on the right, at this position channeling efficiency is very close to 0. The reason of this effect is still to be properly understood, maybe recurring to an X-rays analysis of the crystal in the following months.



For crystals with a bending angle of about $50 \mu\text{rad}$, such as the QM33, a specific analysis of channeling efficiency is required, since the tails of amorphous and channeling peaks overlap, resulting in a not-well distinguished channeling peak. The more the telescope resolution is bad, the more this effect worsens and, in our case, it is visible for the crystal QM33 that has a bending angle of $< 50 \mu\text{rad}$. To solve this ambiguity, there are two different C++ scripts: eff.C, that fits all those crystals with a large banding angle, and eff50.C, thought for crystals like QM33. The latter computes the number of channelled particles as the integral of the Gaussian function that fits the distribution.

BEAM PROPERTIES – December run

The beam parameters during the December measurements were close to those of October: it is indeed possible to recognize the typical tracker resolution values of a pion beam at 180 GeV/c (for x- and y-axes respectively 10.98 μrad and 11.2 μrad), the double Gaussian shape of the beam profiles and the non-Gaussian shape for the beam divergence in y-direction, as shown in **Fig.16a** and **Fig.16b**.

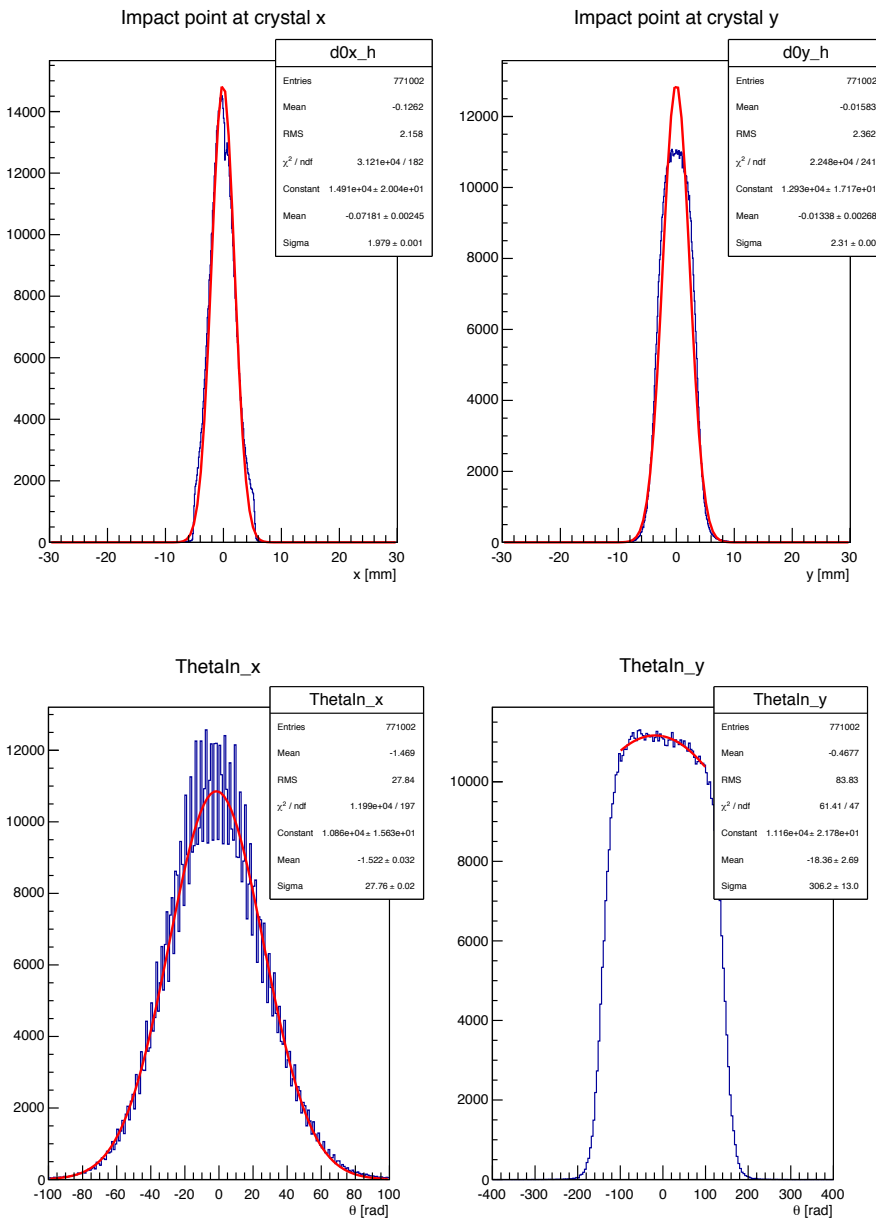


Figure 16a. The plots show the beam dimensions in x- and y- directions. The collimators effect is visible in both of them, especially in x-plot, where at the bottom of the peak doesn't match with the Gaussian fit in red.

Figure 16b. The beam divergence is here reported. As for the case of October, the y-divergence has no Gaussian shape. This is again linked to quadrupole effect on the beam.

MULTISTRIP CRYSTALS

Making an exception for the QM38 and the ST76, which are simple crystals, the test beam run of December was entirely dedicated to measure the multi-strip crystals made by INFN of Ferrara and IHEP laboratories. The final goal was finding the most performing multi-strip to be installed in the SPS pipe.

Crystal name	Crystal type	Manufacture	Bending angle production [μrad]	Length (z) [mm]	Width (x) [mm]	n. of strips
MSTF-13	Multi-Strip	INFN	~500	1.28	1	8
MSTI14-2	Multi-Strip	IHEP	~250	2	0.91	9
MSTI14-4	Multi-Strip	IHEP	~250	2	2	9
MSTI14-5	Multi-Strip	IHEP	unknown	2.5	5	9
MSTI14-6	Multi-Strip	IHEP	~200	2	4	8
QM38	Quasi-Mosaic	PNPI	135	4	5	-
ST76	Strip	INFN	51	4	0.5	simple

Table 2. Basic information of the crystals analyzed in December 2014 TB

The analysis of the multi-strip crystals is different from the simple crystals one, since the attention is focused on the Multiple Volume Reflection (MVR) and not on the channeling effect.

Multiple VR comes from the fact that many particles that undergo to volume capture (VC) in one of the strips take part in volume reflections in the subsequent ones. Such a crystal can be successfully used as a primary collimator for the beam halo collimation of high-energy accelerators.

Since the particles deflection due to volume reflection is small, a way to increase it can be using a sequence of few short bent crystals working in the regime of VR. This possibility has been investigated and it turned out that the beam deflection angles increase proportionally to the number of the strips in the chain.

Differently from channeling effect, VR¹ efficiency is close to 100% and is only limited by volume capture, which brings particles in a channeling regime thanks to the multiple scattering on the atomic nuclei. On the other hand, the beam deflection efficiency should decrease with the rising of reflections number, because of the loss of reflected particles due to volume capture into the channeling states. The beam deflection efficiency due to MVR in N-crystals can be estimated in the first order approximation of independent events as:

$$P_{MVR}(N) = P^N_{VR} = (1 - \epsilon)^N \approx 1 - N\epsilon, \quad \text{where } \epsilon = VR \text{ inefficiency}$$

According to the equation above, the deflection efficiency of 400 GeV/c protons by a sequence of ten silicon strips has been computed to be $\approx 81\%$.

Multi-strips: different technologies

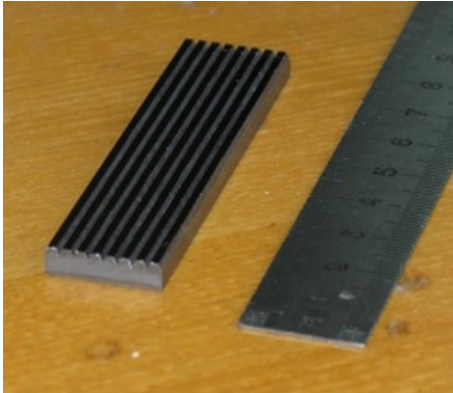
In **Tab.3** are reported the number of strips for each multi-strip crystal and the bending device. It is evident that they are made in different ways: the tested IHEP multi-strips were both typical multi-strips and segments cut on a bent or flat amorphous base.

Crystal name	Manufacture	Bending device	n. of strips
MSTF-13	INFN	Typical multistrip	8*
MSTI14-2	IHEP	Typical multistrip	9
MSTI14-4	IHEP	Segments cut on bent base	9
MSTI14-5	IHEP	Segments cut on thick bent base	9
MSTI14-6	IHEP	Segments cut on a flat base	8

Table 3. Features of multi-strips tested in December.

*MSTF-13 had originally one more strip that broke up during the carriage of the crystal.

¹ VR has been predicted by A. Taratin and S. Vorobiev thirty years before its experimental observation.



The differences between these crystals resulted for the analysis in a specialized technique for geometrical cuts. Actually, for the IHEP crystals whose strips are cut from an amorphous base, the geometrical cuts have to take into account that only the very superficial crystalline planes are involved in MVR, unlike, for instance, the INFN MSTF-13, where the particles interact with the whole crystal width.

Therefore, a trick is needed, i.e. the cut must be done in correspondence of the first crystalline layers and it should be about $100\div200\text{ }\mu\text{m}$.

(To be rigorous, the layers at $50\text{ }\mu\text{m}$ depth give a bigger deflection than those at $100\text{ }\mu\text{m}$ and so on for the entire crystal thickness).

An advantage of multi-strip crystals is that they're easier to align in volume reflection rather than in channeling; moreover we have to consider that the angular acceptance for VR is higher than the channeling one and close to $\sim200\text{ }\mu\text{rad}$.

As touched on in the previous paragraphs, the multi-strip analysis differentiates itself from the simple crystal one, wherefore, while for the latter the main role is played by the High Statistics run, here the attention is focused on the Angular Scan run.

A fine angular scan is thus performed, in order to have a full overview of all the 5 effects highlighted in Fig.4 and to isolate the MVR area.

To choose the most performing crystal for collimation in SPS, the first criterion was identifying the largest multiple volume reflection area in correspondence of which the channeling effect is as low as possible and the deflection is maximum. In other words, we looked for the widest angular range ϑ_x in which the MVR peak is not affected by the presence of channeling spots more than 1%².

Furthermore, the higher are the deflection angle and the MVR efficiency, the better is the crystal.

For all the multi-strips tested in December, the deflection fluctuated in the angular range of $90\div120\text{ }\mu\text{rad}$ for volume reflection, which is not an optimal value, since it must be considered that this angle rescales with $1/\sqrt{E}$, so with 450 GeV/c protons in SPS this definitely drops under $100\mu\text{rad}$.

Figure 17. The first picture above shows an example of IHEP crystal with strips cut on a thick base; the second one is a photo of MSTF-13 installed and aligned with the laser (it is clearly visible the missing strip)

² This percentage is calculated as the number of channelled particles respect to the number of all the particles belonging to that particular angular range.

Angular Scan and MVR efficiency

The analysis path for multi-strips foresees a first look at the plot of deflection_x_vs_d0_x obtained from the high statistics run, exactly as we did for simple strips and QMs, to select the range along the x-axis necessary for the geometrical cuts. Afterwards, these bounds are inserted in torsion_histo.C (a ROOT script that for multi-strips we make run on the Angular Scan run) that returns a plot of the deflection in the horizontal plane in function of the incoming x-angle. Here, we select the appropriated MVR area that responds to the criteria mentioned above by applying an angular cut that at a later stage is needed to get the MVR efficiency (as we have already said, this should be close to 100%).

The following plots show both the angular scans and the multiple volume reflection efficiency for each crystal that was measured in December 2014, where in red we have the Gaussian fit for the MVR peak taken on the mean reflection angle, similarly to what we did for channeling efficiency.

NOTE: the red spotted lines are meant to give only an idea of the angular cuts operated for each crystal. The precise values are reported in **Tab.6**.

MSTF-13

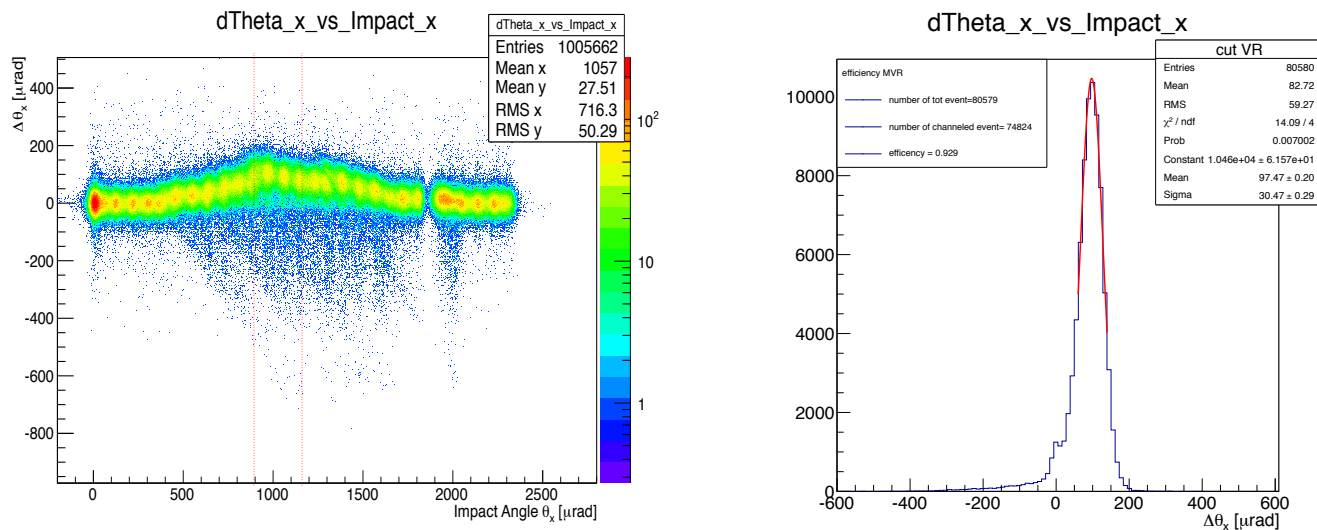


Figure 18a. Angular scan and MVR efficiency for MSTF-13: 0.929, with a deflection angle of 97.47 μrad

MSTI14-2

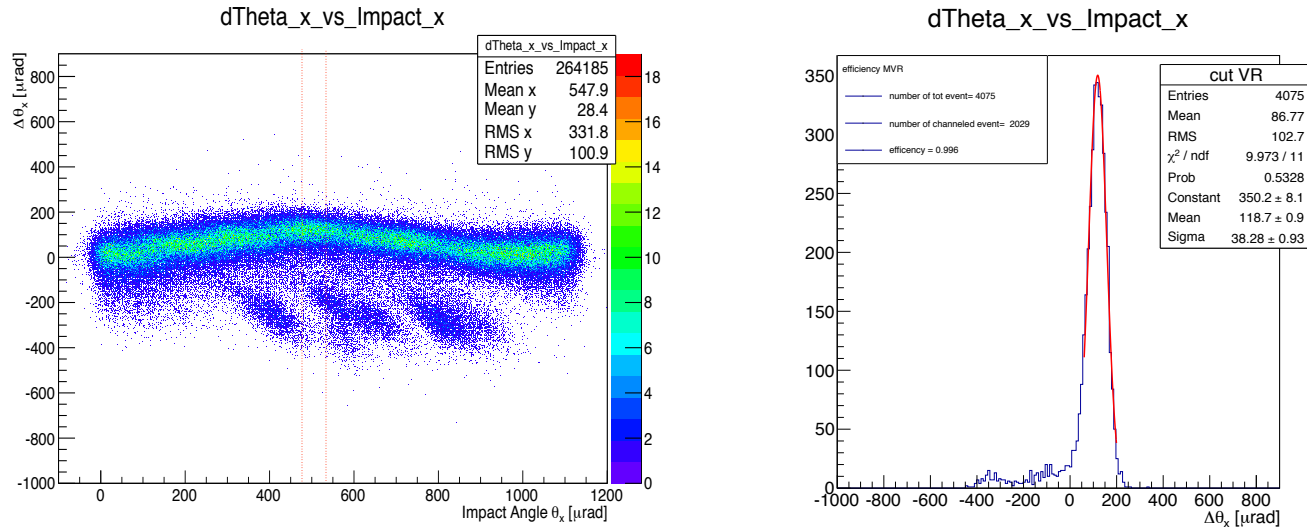


Figure 18b. Angular scan and MVR efficiency for MSTI14-2: 0.996, with a deflection angle of 118.7 μrad

MSTI14-4

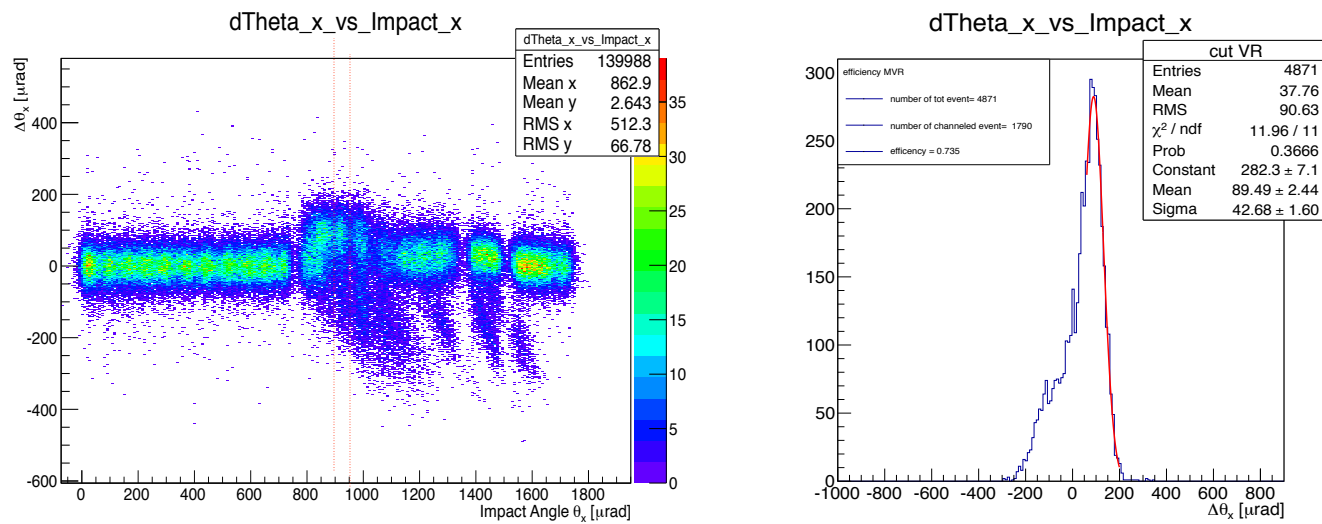


Figure 18b. Angular scan and MVR efficiency for MSTI14-4: 0.735, with a deflection angle of 89.49 μrad

MSTI14-5

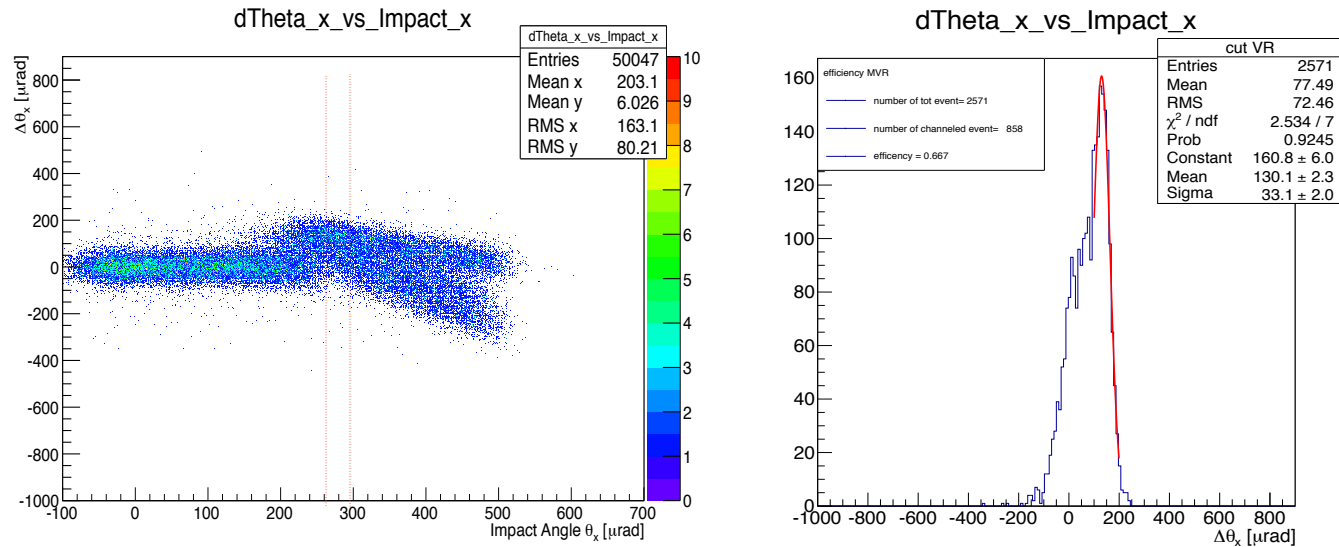


Figure 18c. Angular scan and MVR efficiency for MSTI14-5: 0.667, with a deflection angle of $130.1 \mu\text{rad}$

MSTI14-6

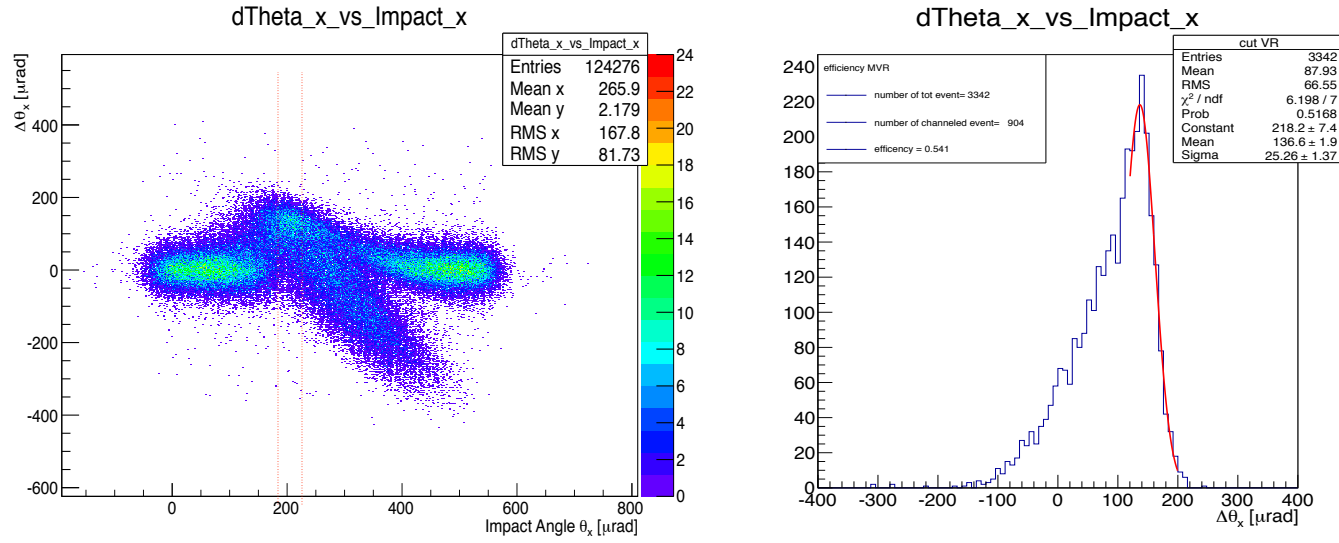


Figure 18d. Angular scan and MVR efficiency for MSTI14-6: 0.541, with a deflection angle of $136.6 \mu\text{rad}$

Other crystals tested in December

Apart from the micro-strips, two more simple crystals were tested in December: ST76 and QM38.

Concerning the strip, it was already measured in the previous test beam, but due to the fact that the bending value found during the offline analysis was pretty far from the predicted one, it has been decided to re-measure it during this second run. What turned out was not only that the production bending angle is too little if compared to the observed one, but this is even bigger than that obtained in October. Moreover, the torsion resulted to be worse as well. The reason behind these two effects is still to be given.

	Bending angle [μrad]	Channeling efficiency		Torsion	
	$\pm 5\mu\text{rad}$	$\pm 10\mu\text{rad}$	$\pm 5\mu\text{rad}$	$\pm 10\mu\text{rad}$	p_0 (offset angle) p_1 (crystal torsion)
October	71.64	70.89	0.635	0.585	3.679 ± 0.6343 -2.71 ± 0.5592
December	81.96	81.26	0.667	0.596	-2.694 ± 0.5727 -5.627 ± 0.5784
Foreseen at fabrication	51				

Table 4. ST76 torsion and bending angle parameters from October and December 2014 test beams

The second crystal is a quasi-mosaic from PNPI. Since this crystal has a quite complicated shape, i.e. it's not an ideal cylinder but a kind of saddle, the bending curvature of the working planes changes from the edge to the deep of the crystal. That's why the efficiency map in function of the x- and y-impact positions has a strong curvature, as shown in **Fig.19**.

Due to this arc-shaped map, it is not possible to apply the geometrical cuts in a way that could identify a sufficient area of constant efficiency, so for this QM, having the same behavior for both the existing high statistics runs, the channeling efficiency has not been computed.

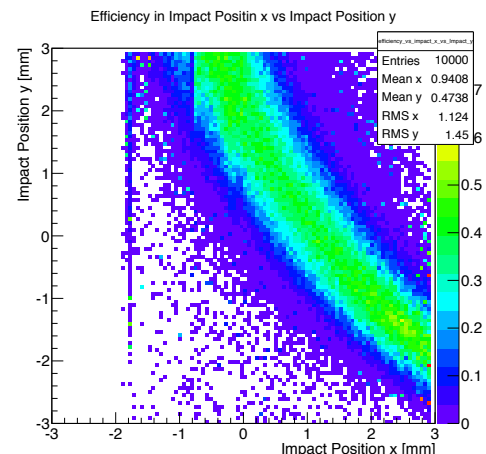


Figure 19. Efficiency map for QM38

CONCLUSIONS

Five simple silicon crystals and five multi-strips plus two more simple crystals were measured respectively in October and December 2014 Test-Beam, at CERN -H8 beam line. Almost all of them have been analysed offline, following the same procedure and taking into account the different parameters that characterize each crystal, starting from the Alignment run, up to the High Statistics run and the Angular Scan run.

The first one gives the beam parameters and ensures the correct alignment of the tracker detectors, while the second, thanks to geometrical and angular cuts (with different methods for strips and quasi-mosaic crystals), allows to compute the torsion correction, the bending angle and the channeling efficiency. Lastly, the latter is of great importance especially for the multi-strip crystals, since it permits to apply to the deflection vs. impact angle plot the angular cuts needed to compute the multiple volume reflection efficiency.

The main parameters resulting from the offline analysis are grouped in the tables above.

Crystal name	Manufacture	Destination	Production bending angle [μrad]	Bending angle [μrad]		Channeling efficiency [%]	
				$\pm 5\mu\text{rad}$	$\pm 10\mu\text{rad}$	$\pm 5\mu\text{rad}$	$\pm 10\mu\text{rad}$
ST9	INFN-Ferrara	SPS	150	120.9	120.8	54.9	49.6
ST76	INFN-Ferrara	LHC	51	71.64	70.89	63.5	58.5
QM33*	PNPI	LHC	44 \pm 2	-37.85	-37.78	62.4	57.1
QM36	PNPI	SPS	170	173.3	173.3	-	-
QM32**	PNPI	SPS	\sim 175	-	-	-	-

Table 5. Summary of the main characteristics found during the offline analysis of October tested crystals.

*QM33 has a negative deflection angle since it has been wrongly installed in its holder; it was re-measured with the positive orientation, giving aligned results.

**QM32 could not be analysed because a problem in reconstructing its High Statistics run

From **Tab.5** we can notice that the two crystals whose purpose is collimation in LHC have the same efficiency for channeling, although their bending angles turned out to be quite distant one from the other. In particular, ST76 has a bending angle bigger than expected from the production measurements.

Instead, concerning the SPS crystals, QM36 has no available values for channeling efficiency because of the defect discovered and described in the previous page, while QM32 could not be analysed because the only high statistics run is too heavy (68 Mevents) and gives reconstruction problems.

Crystal name	Crystal type	Manufacture	Number of strips	Angular cut MVR [μrad]	MVR efficiency	Bending angle [μrad]
MSTF-13	Multi-Strip	INFN	8	900÷1100	0.929	97.47
MSTI14-2	Multi-Strip	IHEP	9	475÷490	0.996	118.7
MSTI14-4	Multi-Strip	IHEP	9	900÷950	0.735	89.68
MSTI14-5	Multi-Strip	IHEP	9	270÷300	0.667	130.1
MSTI14-6	Multi-Strip	IHEP	8	200÷215	0.541	136.6
ST76*	Strip	INFN	1	-	-	81.96/81.26
QM38	Quasi-Mosaic	PNPI	-	-	-	~140**

Table 6. Summary of the main characteristics found during the offline analysis of December tested crystals.

* ST76 has two values for the bending angle because they refer to the cut at $\pm 5 \mu\text{rad}$ and $\pm 10 \mu\text{rad}$.

**The bending value for QM38 is not exact because of the missing efficiency plots. This is due to the strong curvature of the efficiency map reported in Fig.19.

As a consequence of this analysis, two possible candidates that appeared more suitable than the others for installation in SPS have been identified: MSTI14-2 and MSTF13.

Since none of the crystals analyzed has a deflection angle suitable to extract the entire halo in a single turn, the advantage of these two crystals is the possibility to use all the volume of the crystal to obtain volume reflection in a multi-turn regime, which is extremely important to obtain an efficient collimation of the beam.

Between these two crystals, we have decided to install MSTF13 that, in spite of a slightly lower efficiency, provides a larger acceptance for MVR and a greater thickness.